Spin–Orbital Physics in Transition Metal Oxides

Andrzej M. Oleś

Marian Smoluchowski Institute of Physics, Jagellonian University

Reymonta 4, PL-30-059 Kraków, Poland

and Max-Planck-Institut für Festkörperforschung

Heisenbergstr. 1, D-70569 Stuttgart, Germany

We present the main features of the spin–orbital superexchange which describes the magnetic and optical properties of the Mott insulators with orbital degrees of freedom. In contrast to the SU(2) symmetry of spin superexchange, the orbital part of the superexchange obeys the lower cubic symmetry of the lattice and is intrinsically frustrated. This intrinsic frustration and spin–orbital entanglement induce enhanced quantum fluctuations, and we point out a few situations where this leads to disordered states. Strong coupling between the spin and orbital degrees of freedom is discussed on the example of the RVO$_3$ perovskites, with R standing for rare-earth ion, La,...,Lu. We explain the observed evolution of the orbital T_{OO} and Néel T_{N1} transition temperature in the RVO$_3$ series with decreasing ionic radius r_R. A few open problems and the current directions of research in the field of spin–orbital physics are pointed out.

1. Orbital versus spin superexchange

In recent years the physical properties of Mott (or charge transfer) insulators are in the focus of interest in the condensed matter theory [1]. In order to develop theoretical understanding of complex phenomena in doped correlated insulators, including high temperature superconductivity in the cuprates and the colossal magnetoresistance (CMR) in the manganites, it is necessary to describe first the undoped materials, such as La$_2$CuO$_4$ and LaMnO$_3$. In both cases the local Coulomb interactions (Hubbard U) is large and suppresses charge fluctuations, leading to low-energy effective Hamiltonians with superexchange interactions which stabilize antiferromagnetic (AF) spin order at low temperature [2, 3]. However, these two compounds are qualitatively quite different. On the one hand, the degeneracy of partly filled e_g orbitals is lifted in La$_2$CuO$_4$ by the tetragonal distortions of CuO$_6$ octahedra, resulting in two-dimensional (2D) AF superexchange of $S = 1/2$ holes in $x^2 - y^2$ orbitals of Cu^{2+} ions. On the other hand, in LaMnO$_3$ e_g orbital degeneracy plays a fundamental role and, together with the Jahn–Teller (JT) distortions, is required to understand the origin of the anisotropic A-type AF (A-AF) order [4]. As realized already three decades ago [2], in this latter case the orbital degrees of freedom, which are described by the components

$$|x\rangle \equiv \tfrac{1}{\sqrt{2}}\left(x^2 - y^2\right), \quad |z\rangle \equiv \tfrac{1}{\sqrt{2}}\left(3z^2 - r^2\right) \qquad (1)$$

of pseudospin $\tau = 1/2$ and contribute explicitly to the structure of the superexchange. Thus they have to be included on equal footing with ionic spins in a spin–

orbital superexchange model. In the last two decades several new concepts were developed, such as enhanced quantum fluctuations due to orbital degrees of freedom which participate in joint spin–orbital excitations [5], and spin–orbital entanglement which occurs in cases when spin and orbital operators cannot be decoupled from each other [6]. The actual physical problems in this emerging and rapidly developing field were reviewed in the Focus Issue *Orbital Physics* in *New Journal of Physics* [7] a few years ago. Here we want to focus on a few representative recent developments in the field of spin–orbital physics.

Before we will discuss a few consequences of realistic spin–orbital models, let us consider first purely orbital superexchange interactions, as realized in ferromagnetic (FM) 2D systems, such as K$_2$CuF$_4$, or in FM ab planes of three-dimensional (3D) perovskites, either in KCuF$_3$ or in LaMnO$_3$. The superexchange originates from charge $d_i^9 d_j^9 \rightleftharpoons d_i^8 d_j^{10}$ excitations (with $d_i^9 \equiv t_{2g}^6 e_g^3$, $d_i^8 \equiv t_{2g}^6 e_g^2$) in the first case (for Cu^{2+} ions), and from $d_i^4 d_j^4 \rightleftharpoons d_i^3 d_j^5$ (with $d_i^4 \equiv t_{2g}^3 e_g$, $d_i^3 \equiv t_{2g}^3$, and $d_i^5 \equiv t_{2g}^3 e_g^2$) excitations in the second one (for Mn^{3+} ions) [8]. These charge excitations can be transformed away by applying a similar canonical transformation to the one leading to the $t-J$ model [9], commonly used to describe the superconducting cuprates. For the FM compound only high-spin excited states contribute, and in the strong-coupling regime ($t \ll U$) one obtains the effective low-energy Hamiltonian describing orbital superexchange between pseudospins $\tau = 1/2$ due to e_g electrons (holes in KCuF$_3$) in a cubic crystal [5, 10]:

$$\mathcal{H}_0 = H_J + H_z, \tag{2}$$

the first term H_J in Eq. (2) describes superexchange interaction which depends on the superexchange constant

$$J = \frac{4t^2}{U} \tag{3}$$

[here t is the $(dd\sigma)$ hopping element between two $|z\rangle$ orbitals along the c axis, and U is the intraorbital Coulomb interaction], and on Hund's exchange element

$$\eta = \frac{J_{\mathrm{H}}}{U}. \tag{3}$$

This interaction parameterizes the multiplet structure of transition metal ions when anisotropy of the Coulomb and exchange elements is neglected [8]. In the simplest case of d^9 system, the singlet–triplet splitting between the two lowest d^8 excited states is 2η [11].

Following Ref. [10], we will consider below a 3D (perovskite) system with FM spin order and orbital interactions described by the Hamiltonian (2). The origin of intrinsic frustration in the orbital superexchange is best realized by considering its form

$$H_J = \frac{1}{2} J r_1 \sum_{\langle ij \rangle} \left(\tau_i^{(\gamma)} \tau_j^{(\gamma)} - \frac{1}{4} \right), \tag{5}$$

where $\gamma = a, b, c$ refers to the cubic axes, and $r_1 = 1/(1-3\eta)$ follows from the energy of the high-spin charge excitation [8]. The pseudospin operators are defined as follows:

$$\tau_i^{(a,b)} = \frac{1}{4} \left(-\sigma_i^z \pm \sqrt{3}\sigma_i^x \right), \quad \tau_i^{(c)} = \frac{1}{2}\sigma_i^z, \tag{6}$$

where $\sigma_i^{x(z)}$ are the Pauli matrices and sign $+$ $(-)$ is selected for a bond $\langle ij \rangle$ along a (b) axis. The pseudospin interactions $\propto \tau_i^{(\alpha)} \tau_j^{(\alpha)}$ favor alternating orbitals (AOs) on each bond. They are fundamentally different from the SU(2)-symmetric spin interactions, as they: (i) obey only lower cubic symmetry, (ii) are Ising-like, having only one component of the pseudospin interaction which favors pairs of orbitals oriented along the bond (z-like) and in the plane perpendicular to the bond (x-like), and (iii) change their form when the cubic direction is changed. The interactions (5) look to be classical, but in fact due to the form of the pseudospin e_g operators (6) they are not. However, the quantum corrections generated by them are rather small [10].

The second term H_z in Eq. (2) stands for the orbital splitting (by $J\varepsilon_z$), and follows from finite crystal field at either Cu^{2+} or Mn^{3+} ions:

$$H_z = -J\varepsilon_z \sum_i \tau_i^{(c)}. \tag{7}$$

The crystal-field splitting favors electron (hole) occupancy in x (z) orbital for $\varepsilon_z > 0$ or $(\varepsilon_z < 0)$. This term is induced by static distortions in the tetragonal field and is of particular importance in 2D systems, e.g. in the high-T_c cuprates.

The directional nature of pseudospin orbital interactions is responsible for their intrinsic frustration [5, 12]. In fact, the pair of orbitals which would minimize the energy for a bond $\langle ij \rangle$ is different for each cubic axis.

Therefore, while for a single bond the minimal energy of $-\frac{1}{4}J$ can easily be obtained by selecting a pair of orthogonal orbitals on both sites, such as $|z\rangle$ and $|x\rangle$ orbital for a bond along the c axis (let us note that this corresponds to the Ising superexchange interaction as only one orbital is active in intersite charge excitations), this is no longer possible for a 2D (or 3D) system. Thus, unlike in spin systems, the tendency towards disorder (quantum *orbital liquid*) is enhanced with increasing system dimension [13].

The essence of orbital frustration which characterizes the e_g orbital superexchange (5) is captured by the 2D compass model, originally developed as a model for the Mott insulators [2]. Intersite interactions in the compass model are described by products $\tau_i^\alpha \tau_j^\alpha$ of pseudospin components, where $\alpha = x, y, z$, rather than by a scalar product $\boldsymbol{\tau}_i \cdot \boldsymbol{\tau}_j$:

$$\tau_i^x = \frac{1}{2}\sigma_i^x, \quad \tau_i^y = \frac{1}{2}\sigma_i^y, \quad \tau_i^z = \frac{1}{2}\sigma_i^z, \tag{8}$$

where $\alpha = x, y, z$, rather than by a scalar product $\boldsymbol{\tau}_i \cdot \boldsymbol{\tau}_j$. In the 2D case the $\tau_i^x \tau_j^x$ interactions for bonds $\langle ij \rangle$ along the a axis compete with the $\tau_i^z \tau_j^z$ ones along the b axis [14]. Recently certain aspects of this model were investigated by analytic [14] and numerical [15, 16] methods. Despite its closeness to ordinary models used in quantum magnetism, there is no ordered phase with finite magnetization. Thus, this case is qualitatively different from the frustrated Ising interactions on the 2D square lattice, where it was proven rigorously that magnetic order develops below certain transition temperature which depends on the ratio of frustrated to nonfrustrated plaquettes [17]. A competition of pseudospin interactions along different directions results instead in intersite correlations similar to the anisotropic XY model, and competition between two types of Ising-like order generates a quantum phase transition with high degeneracy of the ground state when all interactions have the same strength [15].

It is interesting to note that a similar quantum phase transition exists also in the one-dimensional (1D) compass model [18], when both above interactions alternate along the chain ($N' = N/2$ is the number of unit cells):

$$\mathcal{H}_{1D} = \sum_{i=1}^{N'} \left\{ J_x \tau_{2i-1}^x \tau_{2i}^x + J_z \tau_{2i}^z \tau_{2i+1}^z \right\}. \tag{9}$$

This model was solved exactly in the whole range of $\{J_x, J_z\}$ parameters [18] by mapping to the exactly solvable quantum Ising model [19] in different subspaces (see also this volume [20]). Equal coupling constants $J_x = J_z = J$ correspond to the quantum critical point, where the orbital liquid emerges from two different disordered phases, with hidden order of pairs of pseudospins on every second bond. Presented here 1D model (9) provides thus a beautiful example of a first order quantum phase transition.

2. Spin–orbital models and exotic liquid states

The structure of spin–orbital superexchange involves interactions between SU(2)-symmetric spin scalar products $\boldsymbol{S}_i \cdot \boldsymbol{S}_j$ on each bond $\langle ij \rangle$ connecting two nearest-

-neighbor transition metal ions, each one coupled to or-
bital operators $\{\boldsymbol{\tau}_i, \boldsymbol{\tau}_j\}$ which obey only much lower sym-
metry (at most cubic for a cubic lattice) and its general
form is [8]:

$$\mathcal{H}_J = J \sum_{\langle ij \rangle} \left\{ \hat{\mathcal{J}}_{ij}^{(\gamma)} \left(\boldsymbol{S}_i \cdot \boldsymbol{S}_j + S^2 \right) + \hat{\mathcal{K}}_{ij}^{(\gamma)} \right\}. \qquad (10)$$

The orbital operators $\hat{\mathcal{J}}_{ij}^{(\gamma)}$ and $\hat{\mathcal{K}}_{ij}^{(\gamma)}$ involve the active
orbitals on each bond $\langle ij \rangle$ along direction γ, either e_{g}
or $t_{2\mathrm{g}}$, which participate in $d_i^n d_j^n \rightleftharpoons d_i^{n+1} d_j^{n-1}$ virtual
excitations, and thus have the symmetry of the lattice
(e.g. cubic in the perovskites). The superexchange model
(10) consists of several terms which originate from dif-
ferent charge excitations. This feature made it possible
to relate the averages of these different excitations to the
spectral weights in the optical spectroscopy [21], and this
serves now as a theoretical tool to explain the observed
anisotropy and temperature dependence of the spectral
weights in the optical spectra [8].

The best known spin–orbital model is the Kugel–
Khomskii model for d^9 Cu^{2+} ions which involves the e_{g}
orbital operators (6) and includes both FM and AF spin
interactions, depending on whether the above charge ex-
citation (for $n = 9$) involves the high-spin (triplet) or
one of the low-spin (singlet) d^8 states. These excitations
are parameterized by the coefficients $r_1 = 1/(1 - 3\eta)$,
$r_2 = 1/(1 - \eta)$ and $r_4 = 1/(1 + \eta)$. Using compact nota-
tion of Ref. [11] it can be written as follows:

$$\mathcal{H}_J(d^9) = \tfrac{1}{2} J \sum_{\langle ij \rangle} \left\{ \left[-r_1 \left(\boldsymbol{S}_i \cdot \boldsymbol{S}_j + \tfrac{3}{4} \right) \right. \right.$$
$$\left. + r_2 \left(\boldsymbol{S}_i \cdot \boldsymbol{S}_j - \tfrac{1}{4} \right) \right] \left(\tfrac{1}{4} - \tau_i^{(\gamma)} \tau_j^{(\gamma)} \right)$$
$$+ (r_2 + r_4) \left(\boldsymbol{S}_i \cdot \boldsymbol{S}_j - \tfrac{1}{4} \right) \left(\tfrac{1}{2} - \tau_i^{(\gamma)} \right)$$
$$\left. \times \left(\tfrac{1}{2} - \tau_j^{(\gamma)} \right) \right\}. \qquad (11)$$

In order to derive magnetic excitations for the systems
with orbital degeneracy one usually derives magnetic ex-
change constants for a bond $\langle ij \rangle$ by averaging over the
orbital operators in Eq. (10):

$$J_{ij} = \langle \hat{\mathcal{J}}_{ij}^{(\gamma)} \rangle. \qquad (12)$$

This procedure assumes implicitly that spin and orbital
operators can be decoupled from each other and ig-
nores the possibility of entanglement and composite spin–
orbital excitations introduced in Ref. [5]. It turns out
that such excitations play a prominent role in destabi-
lizing the classical AF long-range order in the d^9 spin–
orbital model [22].

Qualitatively, the classical phase diagram of model (11)
including the crystal-field term (7) consists in the $\{\varepsilon_z, \eta\}$
plane of four AF phases shown schematically in Fig. 1.
First, if η is small, then: (i) if $\varepsilon_z > 0$, the order is AF
and the holes occupy $|x\rangle$ orbitals (2D AFx phase), while
(ii) for $\varepsilon_z < 0$ — $|z\rangle$ orbitals are occupied in the
anisotropic 3D AFz phase. Second, if J_{H}/U is large,
the high-spin excitations become important for the bonds

with different orbitals on both sites, and weak FM inter-
actions ($\propto \eta J$) occur within the ab planes, accompanied
by strong ($\propto J$) AF interactions along the c-axis, leading
to A-AF phase. Depending on the actual value of ε_z, ei-
ther (iii) A-AF1 phase, or (iv) A-AF2 phase (with AF bc
planes and FM bonds along the a axis) is stable on the
classical level. The energies of all the classical phases are
degenerate at the $(\varepsilon_z, \eta) = (0, 0)$ point. The competition
between the above types of spin and orbital order leads
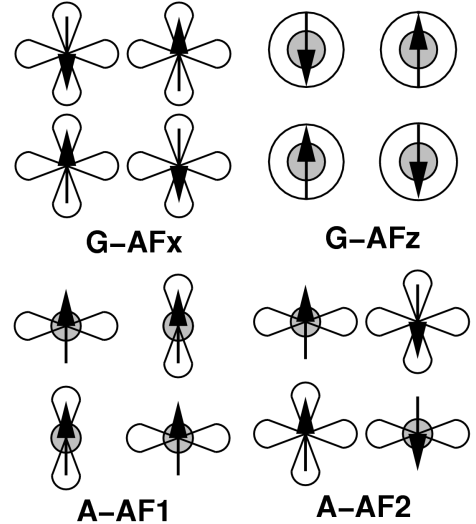here to the quantum critical point at $(\varepsilon_z, \eta) = (0, 0)$.

Fig. 1. Schematic representation of orbital and mag-
netic long-range order in the ab plane of the d^9 model
(11) in: G-AFx, G-AFz, A-AF1, and A-AF2 phase. The
shaded parts of different orbitals are oriented along the
c-axis. The spins (arrows) in the next ab plane along
the c axis are AF to those below them in both G-AFz
and A-AF1 phase, and FM in the A-AF2 phase. In the
G-AFx phase there is no superexchange coupling along
the c axis to the next plane, but this degeneracy is easily
removed when $|x\rangle$ orbitals mix weakly with $|z\rangle$ orbitals.

It has been argued [5, 22] that, similar to the situation
in frustrated $J_1 - J_2 - J_3$ spin models in quantum mag-
netism where the quantum corrections obtained from the
spin-wave theory diverge and suppress the long-range or-
der near quantum critical points [23], the spin order in
all the G-AF and A-AF phases is suppressed near the
$(\varepsilon_z/J, \eta) = (0, 0)$ point. Although counterarguments
were also given that the AFz (but not AFx!) phase
could be stabilized by order-out-of-disorder mechanism
[24] and this controversial issue awaits still an answer
with a more sophisticated treatment, it is believed that
only short-range order with correlations of valence-bond
(VB) type may survive near the transitions between dif-
ferent phases with classical order (Fig. 1). In Ref. [5]
a few representative variational VB wave functions (see
Fig. 2) were constructed, with spin singlets on individ-
ual bonds $\{\langle ij \rangle\}$ accompanied by the variationally opti-
mized orbitals pointing predominantly along the bond.
Each VB phase is characterized by a set K which defines

the bonds $\{\langle ij \rangle\}$ occupied by spin singlets, covering the 3D lattice. The two simplest (dimer) VB states are (see Fig. 2): (i) singlets along the a axis with orbitals close to $3x^2 - r^2$ (VBa phase, degenerate with the analogous VBb phase), (ii) singlets along the c-axis with $|z\rangle$ orbitals (VBc), are indeed more stable than the above classical AF phases, and we emphasize that this happens in three dimensions.
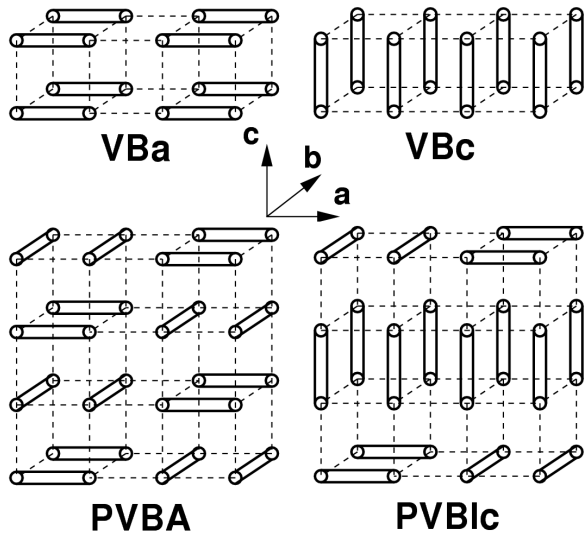

VBa   c   b   a   **VBc**

PVBA   **PVBIc**

Fig. 2. Spin singlets (double lines) in VB states. The singlets along a axis (VBa) or along c axis (VBc) and ordered in either PVBA or PVBIc phase. The axes $\{a, b, c\}$ are shown by arrows.

Further improvement of the energy might be expected by including leading quantum fluctuations in the VB (VBa and VBc) states. In case of the VBa phase this would lead to resonance on each plaquette between the two components composed of spin singlets along the a and b axis, respectively, but this is hindered by the optimized z-like orbitals, oriented in these states either along the a, or along the b axis (therefore the overlap between these two configurations is severely reduced). Unlike in the Heisenberg antiferromagnet, the bonds not occupied by singlets *contribute finite energy* due to the orbital terms similar to those in Sect. 1, and it turns out to be better to optimize the orbital energies due to those bonds depending on whether the bond connects two singlets: either (i) along a single (a, b, or c) axis, or (ii) oriented along two different axes with an angle of $\pi/2$, or (iii) parallel to each other, with the bond making itself an angle of $\pi/2$ to both of them. As the second type of non-singlet bond is energetically the most favorable one, more energy is gained if plaquettes occupied by singlets along a and b axis alternate and form a 3D superlattice, a plaquette VB alternating (PVBA) state (Fig. 2), giving a lower energy than the quantum-corrected A-AF phase. In contrast, the energy of the VBc phase is decreased more by the resonance between the vertical singlets ($\langle ij \rangle \parallel c$). The energy of the result-

ing resonating VBc (RVBc) state could be obtained using the Bethe ansatz result for the 1D Heisenberg antiferromagnet, and adding the orbital energies due to the bonds $\langle ij \rangle \parallel ab$.

Furthermore, a PVB interlayered phase along the c axis (PVBIc), composed of single planes of the PVBA phase interlayered with two planes of VBc vertical singlets (Fig. 2), is more stable in the crossover regime between the RVBc and PVBA phases for $\varepsilon_z < 0$. The orbital energies $\propto J$ in the bonds which connect the singlets on the bonds along the c axis with those lying in the ab planes are then optimized, while the energies $\propto \varepsilon_z$ are gained in the double layers of VBc phase. For $\varepsilon_z > 0$, a rotated interlayered phase (PVBIa) is more stable before the PVBA takes over. Altogether, one finds [5] that an exotic spin–orbital liquid state, represented here by RVBc, PVBIc, PVBIa and PVBA phases, is favored in an extended regime of parameters, in analogy with a 2D 1/5-depleted lattice [25], but the present instability is stronger and happens in a 3D model.

Finally, we remark that the present d^9 model (11) applies also to d^7 low-spin Ni^{3+} ions in LiNiO$_2$ via a particle–hole transformation. However, the situation is rather complex there and also other models were proposed. First, it was argued that a model based on symmetry arguments [26], characterized by a large number of low-lying singlets associated to dimer coverings of the triangular lattice, could explain the properties of LiNiO$_2$. Second, it was shown that charge-transfer terms contribute to the superexchange and they change the balance between different terms in the Hamiltonian, making the orbital interactions stronger than the spin ones [27]. In any case, interplane JT interplane coupling seems to be too weak in LiNiO$_2$ to stabilize the orbital long-range order. The observed difference in the physical properties between NaNiO$_2$ and LiNiO$_2$ remains one of the puzzling phenomena in the field [27] and awaits a future study which has to include all the above aspects.

3. Entanglement in spin–orbital models

Future developments in the theory to understand better the nature of ordered and disordered states in spin–orbital systems have to take into account possible entanglement between both spin and orbital degrees of freedom on the bonds, as for instance in the states of Fig. 2. It is a common wisdom that the magnetism of correlated Mott insulators can be understood by means of the Goodenough–Kanamori rules. They originate from the mean-field (MF) picture and predict that the superexchange interaction between two magnetic ions with degenerate orbitals is strongly AF because of the Pauli principle if the overlap between the occupied orbitals is large, whereas it is weakly FM when the overlap is weak or virtually disappears. This means that spin order and orbital order are complementary — ferro orbital (FO) order supports AF order, while AO order supports FM spin order. Indeed, these celebrated rules are well followed in

the manganites [28, 29], where the AO is robust in the FM ab planes, while the orbitals obey the FO order along the c axis, supporting the AF coupling and leading to the A-AF phase. In fact, one may use here the MF decoupling of the spin and orbital operators, which is sufficient to explain both the magnetic and optical properties of LaMnO$_3$ [8]. The orbital order (or liquid) state determines as well whether the intersite spin correlations are AF or FM in monolayer [30] and in bilayer [31] manganites, while in the perovskite La$_{1-x}$Sr$_x$MnO$_3$ systems the magnons in the FM metallic phase are well explained by the orbital liquid state [32].

As a prominent example of the Goodenough–Kanamori complementarity we would like to mention also the AF phases realized in YVO$_3$ [33], which are the subject of intense research in recent years. While xy orbitals of V^{3+} ions are occupied due to GdFeO$_3$ distortions, the second electron of the d^2 ionic configuration may occupy either yz or zx orbital. Depending on whether these orbitals follow FO or AO order along the c axis, the magnetic correlations are there either AF or FM, explaining the origin of the two observed types of AF order shown in Fig. 3: (i) the C-AF phase, and (ii) the G-AF phase (with AF spin order along all three cubic directions).
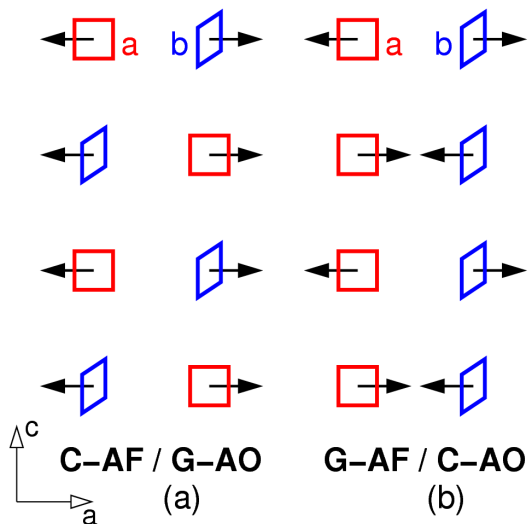

Fig. 3.   Goodenough–Kanamori rules on the example of two AF phases observed in the RVO$_3$ perovskites, with complementary magnetic and orbital order in the ac plane: (a) C-AF spin order accompanied by G-AO order; and (b) G-AF spin order accompanied by C-AO order. Arrows indicate spin order, while squares stand for two active t_{2g} orbitals, a and b. Both spins and orbitals alternate along the b axis (not shown).

One may verify the Goodenough–Kanamori rules by evaluating intersite spin and orbital correlations

$$S_{ij} = \langle \mathbf{S}_i \cdot \mathbf{S}_j \rangle / (2S)^2, \quad T_{ij} = \langle \mathbf{T}_i \cdot \mathbf{T}_j \rangle, \qquad (13)$$

and comparing them with each other. In addition, spin–orbital entanglement can be measured by the composite correlation function defined for a bond $\langle ij \rangle$ [6]:

$$C_{ij} = \frac{\langle (\mathbf{S}_i \cdot \mathbf{S}_j)(\mathbf{T}_i \cdot \mathbf{T}_j) \rangle - \langle \mathbf{S}_i \cdot \mathbf{S}_j \rangle \langle \mathbf{T}_i \cdot \mathbf{T}_j \rangle}{(2S)^2}. \quad (14)$$

When $C_{ij} = 0$, the spin and orbital operators are disentangled and their MF decoupling can be applied, while if $C_{ij} < 0$ — spin and orbital operators are entangled. Let us consider again the structure of spin–orbital superexchange models (10) derived for t_{2g} systems from charge excitations between transition metal ions in configurations: d^1 (Ti^{3+} ions in cubic titanates) with $S = 1/2$ [34], and d^2 (V^{3+} ions in cubic vanadates) with $S = 1$ [35] (for more details about the structure of $\mathcal{H}_J$ in both d^1 and d^2 model see for instance Ref. [8]).

To capture the essence of spin–orbital entanglement it is sufficient to solve t_{2g} models for d^1 and d^2 configurations on four-site chains oriented along the c axis using periodic boundary conditions. One finds entangled spin–orbital states in both models, and nontrivial spin–orbital dynamics strongly influences both intersite spin and orbital intersite correlations (13). In the d^1 (titanate) case one recovers the SU(4) model with $S_{ij} = T_{ij} = C_{ij} = -0.25$ at $\eta = 0$ (Fig. 4a). At finite η the SU(4) degeneracy of all intersite correlations is removed and $T_{ij} < C_{ij} < S_{ij} < 0$, as long as the spin singlet ($S = 0$) ground state persists, i.e., for $\eta < 0.21$. In this regime the Goodenough–Kanamori rule with complementary correlations (implying different signs of S_{ij} and T_{ij}), is violated. Instead, by analyzing the values of the intersite correlations one finds that the ground state wave function for each bond $\langle ij \rangle$ is close to a total spin–orbital singlet, involving a linear combination of (spin singlet/orbital triplet) and (spin triplet/orbital singlet) states. The vanadate d^2 model behaves in a similar way, with all three S_{ij}, T_{ij} and C_{ij} correlations being negative in the spin-singlet ($S = 0$) regime of fluctuating yz and zx orbitals obtained for $\eta < 0.07$ (Fig. 4b). Therefore, the composite spin–orbital correlations are here finite ($C_{ij} < 0$), spin and orbital variables are *entangled*, and the MF factorization of the ground state fails.

To provide further evidence that the Goodenough–Kanamori rules do not apply to t_{2g} systems in the regime of small η, we compare spin exchange constants J_{ij} (12) with the actual values of intersite spin correlations S_{ij} (13). One finds that exchange interaction is formally FM ($J_{ij} < 0$) in the orbital-disordered phase at low values of η (Figs. 4c and d) is in fact accompanied by AF spin correlations ($S_{ij} < 0$), so $J_{ij}S_{ij} > 0$ and the ground state energy calculated in the MF theory is *enhanced* [6]. In contrast, similar analysis (not shown) performed for spin–orbital model (11), derived for d^9 ions with e_g orbital degrees of freedom, gave $J_{ij}S_{ij} < 0$, so here spin correlations follow the sign of the exchange constant [6]. This remarkable difference between t_{2g} and e_g systems originates from composite spin–orbital fluctuations, which are responsible for the *dynamical* nature of exchange constants in the former case. They exhibit large fluctuations around the average value, measured by $\delta J = \{ \langle (\hat{\mathcal{J}}_{ij}^{(\gamma)})^2 \rangle - J_{ij}^2 \}^{1/2}$. As an illustrative example, we give here the values found in the d^1 and d^2 model at
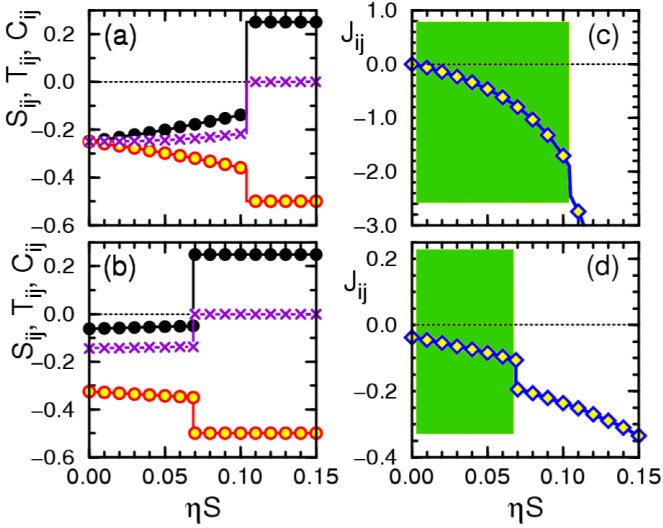
Fig. 4. Left — intersite spin $S_{ij} = \langle \boldsymbol{S}_i \cdot \boldsymbol{S}_j \rangle$ (filled circles), orbital $T_{ij} = \langle \boldsymbol{T}_i \cdot \boldsymbol{T}_j \rangle$ (empty circles), and composite spin–orbital C_{ij} (14) (crosses) correlations for increasing Hund's exchange ηS along c axis; right — the corresponding spin exchange constants J_{ij} (14), as obtained for $N = 4$ site spin–orbital chain (10) with PBC for: (a),(c) d^1 (titanate, $S = 1/2$) model, and (b),(d) d^2 (vanadate, $S = 1$) model. In the shaded areas of (c) and (d) the spin correlations $S_{ij} < 0$ do not follow the sign of the exchange constant $J_{ij} < 0$, and the classical Goodenough–Kanamori rule is violated.

$\eta = 0$. While the average spin exchange constant is small in both cases ($J_{ij} \approx 0$ for d^1, $J_{ij} \approx -0.04$ for d^2), $\hat{\mathcal{J}}_{ij}^{(\gamma)}$ fluctuates widely over both positive and negative values. In the d^1 case the fluctuations between ($S = 0/T = 1$) and ($S = 1/T = 0$) bond wave functions are so large that $\delta J = 1$! They survive even quite far from the high-symmetry SU(4) point (at $\eta > 0.1$), and stabilize spin–orbital singlet phase in a broad regime of η. Also in the d^2 model the orbital bond correlations change dynamically from singlet to triplet, resulting in $\delta J > |J_{ij}|$, with $\delta J = \frac{1}{4}\{1 - (2T_{ij} + \frac{1}{2})^2\}^{1/2} \approx 0.25$, while these fluctuations are small for d^9 model (11) with e_g orbitals.

We emphasize that composite spin–orbital fluctuations which occur in spin–orbital entangled states for realistic parameters determine the magnetic and optical properties of titanates and vanadates. For instance, such composite spin–orbital fluctuations are responsible for the temperature dependence of the optical spectral weights in LaVO$_3$ [21] and trigger spin–orbital dimerization in the C-AF phase of YVO$_3$ in the intermediate temperature regime (see below) [36]. Remarkably, the observed dimerization in the magnetic excitations may be seen as a signature of entanglement in excited states which become relevant at finite temperature. It is activated by thermal fluctuations in the spin chain [37], which couple to dimerized correlations in the orbital sector.

4. Phase transitions in the RVO$_3$ perovskites

Recent progress in experimental studies of transition metal oxides provided exceptionally detailed information on the phase diagrams of the RMnO$_3$ manganites [38] and the RVO$_3$ vanadates [39] (where R = La, Pr,..., Lu). In the manganites the orbital order appears first when the temperature is lowered (at $T_{OO} \approx 800$ K), and its onset is accompanied by a lattice distortion. The magnetic order follows at much lower temperature $T_N \approx 140$ K. This separation of the spin and orbital energy scales follows also from the JT distortions which contribute to the orbital interactions and enhance the value of T_{OO} [4]. Recent experiments showed that the orbital transition temperature T_{OO} is enhanced when the ionic radius r_R of the R^{3+} ions decreases along the RMnO$_3$ perovskites, while T_N is drastically reduced, resulting in the change of magnetic order from the A-AF to the E-AF phase [38]. This behavior could not be understood until now and is one of the challenges for the theory.

The experimental situation in the cubic vanadates is different and even more complex. On the one hand, the magnetic order in YVO$_3$ is G-AF (Fig. 5b) at low temperature, and changes at the first order magnetic transition at $T_{N2} = 77$ K to the C-AF structure, which remains stable up to $T_{N1} \approx 116$ K. The magnetic transition at T_{N2} is particularly surprising as the staggered moments change their direction from approximately parallel to the c axis in the G-AF phase to lying almost within the ab planes in the C-AF phase, with some small alternating G-AF component [40]. Although it was argued that the entropy due to magnetic and orbital excitations is higher in the C-AF phase [35, 41], the magnetization reversal at the lower magnetic transition remains mysterious, and this phenomenon is still puzzling and far from being completely understood. On the other hand, only the C-AF order develops in LaVO$_3$ below a somewhat higher $T_{N1} \approx 143$ K, and is almost immediately followed by a weak structural transition stabilizing the weak G-AO order at $T_{OO} \approx 141$ K [39, 42] (Fig. 5a). Remarkably, the magnetic order parameter in the C-AF phase of LaVO$_3$ is strongly reduced to ≈ 1.3 μ_B, much below the reduction expected from quantum fluctuations in the C-AF phase (being only 6% for $S = 1$ spins) [43] — also this reduction of the measured magnetization could not be explained so far.

Experimental studies have shown that the C-AF order is common to the entire family of the RVO$_3$ vanadates, and in general $T_{N1} < T_{OO}$, except for LaVO$_3$ with $T_{N1} \approx T_{OO}$ [39, 42]. When the ionic radius r_R decreases, the Néel temperature T_{N1} also decreases, while orbital transition temperature T_{OO} increases, passes through a maximum close to YVO$_3$, and decreases again towards LuVO$_3$. Knowing that orbital quantum fluctuations and spin–orbital entanglement play so important role in the perovskite vanadates, it is of interest to ask whether the spin–orbital model of the form (10) introduced for the perovskite vanadates [35, 36] is able to describe this variation of T_{OO} and T_{N1} with decreasing radius r_R of R

ions in RVO$_3$ [39]. It is clear that the nonmonotonic dependence of $T_{\rm OO}$ on $r_{\rm R}$ cannot be reproduced just by the superexchange, as it requires two mechanisms which oppose each other. In fact, there is even no reason to assume that the superexchange constant J should depend on $r_{\rm R}$, as the distances between V^{3+} ions are quite close to each other in different compounds [44–46], so neither t nor U is expected to change significantly.

As in the RMnO$_3$ manganites [38], one expects that the JT distortions should increase when the ionic radius $r_{\rm R}$ decreases, and one could argue that this would induce the increase in $T_{\rm OO}$. In order to unravel the physical mechanism responsible for the decrease in $T_{\rm OO}$ from YVO$_3$ to LuVO$_3$ one has to analyze in more detail the evolution of GdFeO$_3$ distortions with decreasing $r_{\rm R}$ [47]. Such distortions are common for the perovskites [48], and may be described by two subsequent rotations of VO$_6$ octahedra: (i) by an angle ϑ around the b axis, and (ii) by an angle φ around the c axis. Increasing angle ϑ causes a decrease in V–O–V bond angles along the c direction, being $\pi - 2\vartheta$, and leads to an orthorhombic lattice distortion $u = (b - a)/a$, where a and b are the lattice parameters of the *Pbnm* structure of RVO$_3$. The structural data for the perovskite RVO$_3$ vanadates [44–46] give the following empirical relation between the ionic radius $r_{\rm R}$ and the angle ϑ:

$$r_{\rm R} = r_0 - \alpha \sin^2 \vartheta, \qquad (15)$$

where $r_0 = 1.5$ Å and $\alpha = 0.95$ Å. This allows one to use the angle ϑ to parameterize the dependence of the microscopic parameters and the transition temperatures $T_{\rm OO}$ and $T_{\rm N1}$ on $r_{\rm R}$.

The spin–orbital model introduced in Ref. [47] to describe the phase diagram of RVO$_3$ includes: (i) the superexchange $\propto J$ between V^{3+} ions in the d^2 configuration with $S = 1$ spins [35], (ii) the crystal-field splitting $\propto E_z$ between yz and zx orbitals, (iii) intersite orbital interactions $\propto V_{ab}, V_c$ (which originate from the coupling to the lattice), and (iv) orbital-lattice term which induces orbital polarization when the distortion u increases. The Hamiltonian consists thus of several terms [47]:

$$\mathcal{H} = J \sum_{\langle ij \rangle \| \gamma} \left[\left(\boldsymbol{S}_i \cdot \boldsymbol{S}_j + S^2 \right) \mathcal{J}_{ij}^{(\gamma)} + \mathcal{K}_{ij}^{(\gamma)} \right]$$
$$+ E_z(\vartheta) \sum_i \mathrm{e}^{\mathrm{i} \boldsymbol{R}_i \boldsymbol{Q}} \tau_i^z - V_c(\vartheta) \sum_{\langle ij \rangle \| c} \tau_i^z \tau_j^z$$
$$+ V_{ab}(\vartheta) \sum_{\langle ij \rangle \| ab} \tau_i^z \tau_j^z$$
$$- gu \sum_i \tau_i^x + \tfrac{1}{2} N K [u - u_0(\vartheta)]^2, \qquad (16)$$

with $\gamma = a, b, c$ labeling the cubic axes. The orbital operators take the form

$$\hat{\mathcal{J}}_{ij}^{(\gamma)} = \tfrac{1}{2} \left[(1 + 2\eta r_1) \left(\boldsymbol{\tau}_i \cdot \boldsymbol{\tau}_j + \tfrac{1}{4} n_i n_j \right) \right.$$
$$\left. - \eta r_3 \left(\boldsymbol{\tau}_i \times \boldsymbol{\tau}_j + \tfrac{1}{4} n_i n_j \right) - \tfrac{1}{2} \eta r_1 (n_i + n_j) \right]^{(\gamma)}, \quad (17)$$

$$\hat{K}_{ij}^{(\gamma)} = [\eta r_1 \left(\boldsymbol{\tau}_i \cdot \boldsymbol{\tau}_j + \tfrac{1}{4} n_i n_j \right) + \eta r_3 \left(\boldsymbol{\tau}_i \times \boldsymbol{\tau}_j + \tfrac{1}{4} n_i n_j \right)$$

$$- \tfrac{1}{4} (1 + \eta r_1)(n_i + n_j)]^{(\gamma)}, \qquad (18)$$

and have a rich structure which originates from the projections of the d_i^3 excited states on the respective eigenstates of V^{2+} ion. They arise due to the $d_i^2 d_j^2 \rightleftharpoons d_i^3 d_j^1$ charge excitations, leading either to high-spin or to low-spin d_i^3 configurations, so Hund's exchange splittings in the multiplet structure of V^{2+} ions enter via the coefficients $r_1 = 1/(1 - 3\eta)$ and $r_3 = 1/(1 + 2\eta)$ (the lower energy singlet excitations occur at energy U, so the corresponding coefficient is $r_2 = 1$). Using the atomic value of Hund's exchange, we have estimated that $\eta \approx 0.13$ [8, 41]. The orbital operators $\boldsymbol{\tau}_i = \{\tau_i^+, \tau_i^-, \tau_i^z\}$ for pseudospin $\tau = 1/2$ in Eqs. (17) and (18) are defined in the subspace spanned by two orbital flavors which are active along a given cubic direction $\gamma = a, b, c$. Unlike in d^9 model (11) for e_g orbitals, the leading orbital interactions are here proportional to the scalar products $(\boldsymbol{\tau}_i \cdot \boldsymbol{\tau}_j)^{(\gamma)}$ of orbital operators on the bonds, but the structure of local Coulomb interactions is responsible for additional terms

$$(\boldsymbol{\tau}_i \times \boldsymbol{\tau}_j)^{(\gamma)} = \tfrac{1}{2} \left(\tau_i^+ \tau_j^+ + \tau_i^- \tau_j^- \right) + \tau_i^z \tau_j^z, \qquad (19)$$

so the orbital quantum numbers are not conserved. Finally, the operator $n_i^{(\gamma)}$ stands for the number of active electrons at site i along the bond $\langle ij \rangle$, for instance for a bond along the c axis this number is $n_i^{(c)} = n_{i,yz} + n_{i,zx}$.

Further insight into the electronic configuration on V^{3+} ions in RVO$_3$ may be obtained either by investigating the electronic structure [49], or by explicit calculations using the point charge model [47]. Both lead to the electronic configurations $(xy)^1(yz/zx)^1$, i.e., the xy orbitals are occupied at all sites, while the remaining $\{yz, zx\}$ orbitals represent active orbital degrees of freedom which contribute to the t_{2g} orbital dynamics, expressed by the scalar product $\boldsymbol{\tau}_i \cdot \boldsymbol{\tau}_j$ (only for $\gamma \equiv c$). This demonstrates an important difference between the e_g (with one electron or one hole in e_g orbitals at each site) and a t_{2g} system, such as the RVO$_3$ perovskites. Two active t_{2g} orbitals along this bond open a new possibility — if both orbitals are singly occupied, an *orbital singlet* gives here FM superexchange, even in the absence of Hund's exchange (at $\eta = 0$) [35].

Furthermore, the actual electronic configurations realized in the RVO$_3$ systems justify the form of the crystal-field term used in Eq. (16), with $\tau_i^z = \tfrac{1}{2}(n_{i,yz} - n_{i,zx})$. The crystal field alternates in the ab planes, but is uniform along the c axis. It is thus characterized by the vector $\boldsymbol{Q} = (\pi, \pi, 0)$ in reciprocal space, and competes with the (weak) G-AO order supporting the observed C-AF phase below $T_{\rm N1}$. The orbital interactions induced by the distortions of the VO$_6$ octahedra and by GdFeO$_3$ distortions of the lattice, $V_{ab} > 0$ and $V_c > 0$, also favor the C-AO order (like $E_z > 0$). Let us note that $V_c > 0$ counteracts the orbital interactions included in the superexchange. In case of V_c one may assume that its dependence on the angle ϑ is weak, and a constant $V_c(\vartheta) = 0.26J$ was chosen in Ref. [47] in order to satisfy the experimental condition that the C-AF and G-AO order appears almost simultaneously in LaVO$_3$, see Fig. 5a.
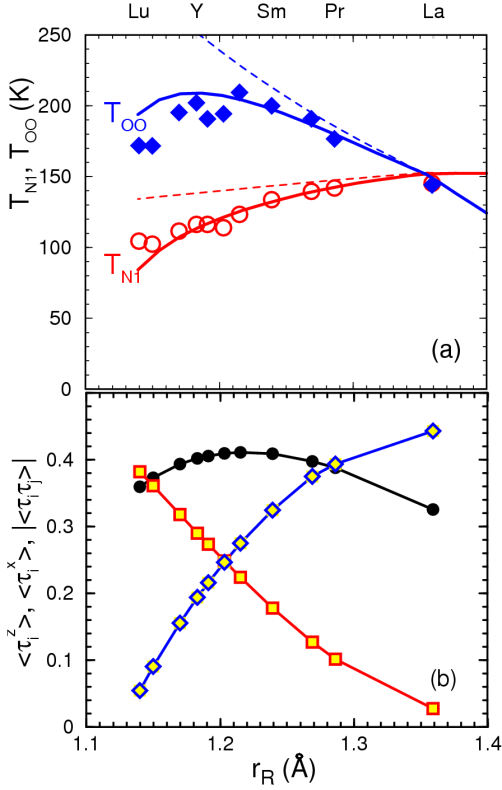
Fig. 5. Theoretical description of orbital and magnetic phase transition in the RVO$_3$ perovskites obtained using model (16), for varying ionic radius r_R of R ions: (a) transition temperatures — T_{OO} for the onset of orbital and T_{N1} for the onset of the C-AF order, as obtained in Ref. [47] (solid lines), and compared with the experimental data of Ref. [39] (filled diamonds and open circles); (b) evolution of orbital order parameter $\langle\tau_i^z\rangle_G$ (filled circles), transverse orbital polarization $\langle\tau_i^x\rangle$ (squares), and orbital intersite correlations $|\langle\boldsymbol{\tau}_i\cdot\boldsymbol{\tau}_j\rangle|$ (diamonds) along c axis at $T = 0$. Parameters: $J = 200$ K, $v_z = 17$, $v_{ab} = 22$, $v_g = 740$.

The experimental value $T_{N1}^{\exp} = 143$ K for LaVO$_3$ [39] was fairly well reproduced in the present model taking $J = 200$ K. The functional dependence of the remaining two parameters $\{E_z, V_{ab}\}$ on the tilting angle ϑ was derived from the point charge model [47], using the structural data for RVO$_3$ [44–46]. In this way the following two relations were deduced:

$$E_z(\vartheta) = Jv_z\sin^3\vartheta\cos\vartheta, \tag{20}$$

$$V_{ab}(\vartheta) = Jv_{ab}\sin^3\vartheta\cos\vartheta. \tag{21}$$

The last two terms in Eq. (16) describe the linear coupling $\propto g > 0$ between active $\{yz, zx\}$ orbitals and the orthorhombic lattice distortion u. The elastic energy which counteracts lattice distortion u is given the force constant K, and N is the number of V^{3+} ions. The coupling $\propto gu$ acts as a transverse field in the pseudospin space. While the eigenstates $\frac{1}{\sqrt{2}}(|yz\rangle \pm |zx\rangle)$ favored by τ_i^x cannot be realized due to the competition with all the

other terms, increasing lattice distortion u (increasing angle ϑ) modifies the orbital order and intersite orbital correlations. At the minimum one finds an effective coupling

$$g_{\text{eff}}(\vartheta; T) \equiv gu(\vartheta; T) = gu_0(\vartheta) + \frac{g^2}{K}\langle\tau^x\rangle_T, \tag{22}$$

with the global distortion $u(\vartheta; T)$ caused by (i) a pure lattice term $u_0(\vartheta)$, and (ii) an orbital contribution $\propto \langle\tau^x\rangle$ which can be determined self-consistently within the present approach, see Ref. [47]. Both u_0 and $\langle\tau^x\rangle$ are expected to increase with increasing tilting ϑ. This dependence has to be faster than the ones of Eqs. (20) and (21), as otherwise no maximum in the dependence of T_{OO} on r_R would be obtained. Using this argument a semiempirical relation

$$g_{\text{eff}}(\vartheta) = Jv_g\sin^5\vartheta\cos\vartheta, \tag{23}$$

was postulated in Ref. [47]. Therefore, magnetic and orbital correlations described by spin–orbital model (10) depend on three parameters: $\{v_z, v_{ab}, v_g\}$.

While the above fast dependence on the tilting angle ϑ of VO$_6$ octahedra in the RVO$_3$ family was introduced in order to reproduce the experimentally observed dependence of T_{OO} on r_R, see Fig. 5a, it may be justified *a posteriori*. It turns out that the dependence of g_{eff} on the ionic radius r_R follows the actual lattice distortion u in RVO$_3$ measured at $T = 0$ (or just above T_{N1}) [47]. Also the orbital polarization $\langle\tau^x\rangle$ is approximately $\propto \sin^5\vartheta\cos\vartheta$, and follows the same fast dependence of $g_{\text{eff}}(\vartheta)$ for the RVO$_3$ perovskites. These results indicate that the bare coupling parameters $\{g, K\}$ are nearly constant and independent of r_R, which may be treated as a prediction of the theory to be verified by future experiments.

Similar to the RMnO$_3$ manganites [4], the correct MF treatment of the orbital and magnetic phase transitions in the RVO$_3$ vanadates requires the coupling between the on-site orbital, $\langle\tau^z\rangle_G \equiv \frac{1}{2}|\langle\tau_i^z - \tau_j^z\rangle|$, and spin, $\langle S_i^z\rangle_C$, order parameters in the C-AF phase, as well as a composite $\langle S_i^z\tau_i^z\rangle$ order parameter. Unlike in the perovskite manganites [38], however, the on-site MF theory does not suffice for the RVO$_3$ compounds as the orbital singlet correlations $\langle\boldsymbol{\tau}_i \cdot \boldsymbol{\tau}_j\rangle$ on the bonds $\langle ij\rangle$ along the c axis play an important role in stabilizing the C-AF phase [35, 41]. Therefore, the minimal physically acceptable approach to the present problem is a self-consistent calculation for a bond $\langle ij\rangle$ along the c axis, embedded in the MF terms due to its neighbors along all the cubic axes [47]. This procedure, with properly selected model parameters, served to reproduce the experimental phase diagram of Fig. 5a. One finds that the orbital transition occurs first in the RVO$_3$ vanadates with $r_R < r_{La}$, as observed. At the same time, the Néel temperature T_{N1} decreases with decreasing r_R.

The key feature of the present spin–orbital system which drives the observed dependence of T_{OO} and T_{N1} on the ionic radius r_R is the evolution of intersite orbital correlations $\langle\boldsymbol{\tau}_i \cdot \boldsymbol{\tau}_j\rangle$ along the c axis, and the increasing

orbital polarization $\langle\tau^x\rangle$ with decreasing r_R (Fig. 5b). Indeed, the singlet correlations are drastically suppressed from LaVO$_3$ towards LuVO$_3$. While $\langle\tau^x\rangle \approx 0.03$ is rather weak in LaVO$_3$, it steadily increases along the RVO$_3$ perovskites when r_R decreases, and finally it becomes as important as the orbital order parameter, $\langle\tau^x\rangle \approx \langle\tau^z\rangle_G$. Let us note that in all the cases the latter order parameter is substantially reduced from the classical value $\frac{1}{2}$ by singlet orbital fluctuations, being $\langle\tau^z\rangle_G \approx 0.32$ and 0.36 for LaVO$_3$ and LuVO$_3$, respectively.

The results presented in Ref. [47] demonstrate the remarkable dependence of both spin and orbital order on the orbital correlations. First, the increase in orbital intersite interactions due to the JT term (21), induces steady increase in the orbital temperature T_{OO} with decreasing r_R. When the orbital polarization $\langle\tau^x\rangle$ becomes large, however, this increase is suppressed and one reproduces the nonmonotonic dependence of T_{OO} on r_R, with the observed drop of T_{OO} when r_R decreases beyond $r_R \approx 1.18$ Å of YVO$_3$. Second, the changes in intersite orbital correlations shown in Fig. 5b modify the magnetic exchange constants $\{J_{ab}, J_c\}$ along the bonds parallel to one of cubic directions in the ab planes or along the c axis (12), and thus the value of T_{N1} is reduced with decreasing r_R, although the superexchange energy J does not change. This also means that the width of the magnon band given at $T = 0$ by $W_{C-AF} = 4(J_{ab} + |J_c|)$ [41] is reduced by a factor close to 1.8 from LaVO$_3$ to YVO$_3$, in agreement with surprisingly low magnon energies observed in the C-AF phase of YVO$_3$ [33].

Summarizing, spin–orbital model (16) of Ref. [47] provides an almost quantitative understanding of the systematic experimental trends for both orbital and magnetic transitions in the RVO$_3$ perovskites, and is able to reproduce the nonmonotonic variation of the orbital temperature T_{OO} for decreasing r_R. Hovever, the theoretical description of the magnetic transition to the G-AF phase at T_{N2}, which occurs for small r_R [39], remains to be addressed by future theory. More open issues and future directions of reasearch in the field of the orbital physics are shortly indicated in the next section.

5. Summary and open problems

A few representative problems discussed above demonstrate that the spin–orbital physics is a very rich field, with intrinsically frustatred interactions and rather exotic ordered or disordered phases, and with their behavior frequently dominated by quantum fluctuations. While valuable information about the electronic structure is obtained from density functional theory [50], the many-body aspects have to be studied using models of correlated electrons. Perhaps the most important feature of orbital or spin–orbital superexchange models is strong coupling between the orbitals and the lattice, which may help to stabilize orbital order, as in model (16) introduced for the RVO$_3$ perovskites [47]. In this way, the lattice distortions may also indirectly influence the onset of magnetic order in systems with active orbital degrees of freedom. If they are absent and the lattice is frustrated in addition, a very interesting situation arises, with strong tendency towards truly exotic quantum states [51]. Examples of this behavior were considered recently for the triangular lattice, both for e_g orbitals in LiNiO$_2$ [27] and t_{2g} orbitals in NaTiO$_2$ [52]. None of these models could really be solved, but generic tendency towards dimer correlations with spin singlets on the bonds for particular orbital states could be shown.

Rapid progress in the field of orbital physics results mainly from developing new experimental techniques and synthesizing novel materials. While the experiment is ahead of the theory in most cases, there are some exceptions. One of them was a theoretical prediction of the energy and dispersion of orbital excitations [10, 53]. Only recently orbital excitations (orbitons) could be observed in the Raman scattering in the Mott insulators LaTiO$_3$ and YTiO$_3$ [54]. An interesting question which arises in this context is carrier propagation in a Mott insulator with AO order. This problem is very complex and has been addressed also in the last decade of the previous century [55]. Not only spin excitations may provide more final states, as for triplet excitations in the $t-J$ model [56], but a carrier may dress by orbital excitations [57], and scatter on magnons [58]. Indeed, the coupling to orbitons increases the effective mass of a moving hole in e_g systems [57]. The orbital part of the superexchange is classical t_{2g} systems, but also there weak quasiparticle dispersion arises from three-site processes [59] (for more details see also recent Ref. [60]).

Similar to doped manganites [61], also in doped R$_{1-x}$(Sr,Ca)$_x$VO$_3$ systems orbital order gradually disappears [62]. The composite C-AF/G-AO order survives, however, is a broad range of doping, in contrast to La$_{1-x}$Sr$_x$MnO$_3$, where FM order sets in already at $x \approx 0.10$. It is quite remarkable that the complementary G-AF/C-AO type of order is fragile and disappears in Y$_{1-x}$Ca$_x$VO$_3$ already at $x = 0.02$ [62]. We remark that the holes doped in C-AF/G-AO phase are localized in polaron-like states [63], so the purely electronic model such as of Ref. [59] is too crude to capture both the evolution of the spin–orbital order in doped vanadates and the gradual decrease in the energy scale for spin–orbital fluctuations.

As a final remark, we would like to mention very promising recent experimental studies of Ni-based superlattices [64]. Recent theory for LaNiO$_3$/LaMO$_3$ superlattices (with M = Al, Gd, Ti) [65] predicts that the correlated e_g electrons in the NiO$_2$ planes develop a planar $x^2 - y^2$ orbital order driven by the reduced dimensionality and further supported by epitaxial strain from the substrate. This resembles the $x^2 - y^2$ orbital polarization in doped layered manganites [66]. As in all other cases discussed above, the superexchange interactions which involve the orbital degrees of freedom play here a crucial role to understand the observed magnetic order and low-lying excited states.

Acknowledgments

References

[1] M. Imada, A. Fujimori, Y. Tokura, *Rev. Mod. Phys.* **70**, 1039 (1998).

[2] K.I. Kugel, D.I. Khomskii, *Sov. Phys. Usp.* **25**, 231 (1982).

[3] C. Castellani, C.R. Natoli, J. Ranninger, *Phys. Rev. B* **18**, 4945 (1978); **18**, 4967 (1978); **18**, 5001 (1978).

[4] L.F. Feiner, A.M. Oleś, *Phys. Rev. B* **59**, 3295 (1999).

[5] L.F. Feiner, A.M. Oleś, J. Zaanen, *Phys. Rev. Lett.* **78**, 2799 (1997).

[6] A.M. Oleś, P. Horsch, L.F. Feiner, G. Khaliullin, *Phys. Rev. Lett.* **96**, 147205 (2006).

[7] B. Keimer, A.M. Oleś, *Focus on Orbital Physics, New J. Phys.* **6**, E05 (2004).

[8] A.M. Oleś, P. Horsch, G. Khaliullin, L.F. Feiner, *Phys. Rev. B* **72**, 214431 (2005).

[9] K.A. Chao, J. Spałek, A.M. Oleś, *J. Phys. C* **10**, L271 (1977).

[10] J. van den Brink, F. Mack, P. Horsch, A.M. Oleś, *Phys. Rev. B* **59**, 6795 (1999).

[11] A.M. Oleś, L.F. Feiner, J. Zaanen, *Phys. Rev. B* **61**, 6257 (2000).

[12] J. van den Brink, *New J. Phys.* **6**, 201 (2004).

[13] L.F. Feiner, A.M. Oleś, *Phys. Rev. B* **71**, 144422 (2005).

[14] D.I. Khomskii, M.V. Mostovoy, *J. Phys. A* **36**, 9197 (2003).

[15] J. Dorier, F. Becca, F. Mila, *Phys. Rev. B* **72**, 024448 (2005).

[16] S. Wenzel, W. Janke, *Phys. Rev. B* **78**, 064402 (2008).

[17] L. Longa, A.M. Oleś, *J. Phys. A* **13**, 1031 (1980).

[18] W. Brzezicki, J. Dziarmaga, A.M. Oleś, *Phys. Rev. B* **75**, 134415 (2007).

[19] J.H.H. Perk, H.W. Campel, G.R.W. Quispel, F.W. Nijhoff, *Physica A* **123**, 1 (1984).

[20] W. Brzezicki, A.M. Oleś, *Acta Phys. Pol. A* **115**, 162 (2009).

[21] G. Khaliullin, P. Horsch, A.M. Oleś, *Phys. Rev. B* **70**, 195103 (2004).

[22] L.F. Feiner, A.M. Oleś, J. Zaanen, *J. Phys., Condens. Matter* **10**, L555 (1997).

[23] P. Chandra, B. Douçot, *Phys. Rev. B* **38**, 9335 (1988).

[24] G. Khaliullin, V. Oudovenko, *Phys. Rev. B* **56**, 14243(R) (1997).

[25] K. Ueda, H. Kontani, M. Sigrist, P.A. Lee, *Phys. Rev. Lett.* **76**, 1932 (1996).

[26] F. Vernay, K. Penc, P. Fazekas, F. Mila, *Phys. Rev. B* **70**, 014428 (2004).

[27] A.J.W. Reitsma, L.F. Feiner, A.M. Oleś, *New J. Phys.* **7**, 121 (2005).

[28] A. Weiße, H. Fehske, *New J. Phys.* **6**, 158 (2004).

[29] E. Dagotto, *New J. Phys.* **7**, 67 (2005).

[30] M. Daghofer, W. von der Linden, A.M. Oleś, *Phys. Rev. B* **70**, 184430 (2004).

[31] M. Daghofer, A.M. Oleś, D.M. Neuber, W. von der Linden, *Phys. Rev. B* **73**, 104451 (2006).

[32] A.M. Oleś, L.F. Feiner, *Phys. Rev. B* **65**, 052414 (2002).

[33] C. Ulrich, G. Khaliullin, J. Sirker, M. Reehuis, M. Ohl, S. Miyasaka, Y. Tokura, B. Keimer, *Phys. Rev. Lett.* **91**, 257202 (2003).

[34] G. Khaliullin, S. Maekawa, *Phys. Rev. Lett.* **85**, 3950 (2000).

[35] G. Khaliullin, P. Horsch, A.M. Oleś, *Phys. Rev. Lett.* **86**, 3879 (2001).

[36] P. Horsch, G. Khaliullin, A.M. Oleś, *Phys. Rev. Lett.* **91**, 257203 (2003).

[37] J. Sirker, A. Herzog, A.M. Oleś, P. Horsch, *Phys. Rev. Lett.* **101**, 157204 (2008).

[38] J.-S. Zhou, J.B. Goodenough, *Phys. Rev. Lett.* **96**, 247202 (2006).

[39] S. Miyasaka, Y. Okimoto, M. Iwama, Y. Tokura, *Phys. Rev. B* **68**, 100406 (2003).

[40] Y. Ren, T.T.M. Palstra, D.I. Khomskii, A.A. Nugroho, A.A. Menovsky, G.A. Sawatzky, *Phys. Rev. B* **62**, 6577 (2000).

[41] A.M. Oleś, P. Horsch, G. Khaliullin, *Phys. Rev. B* **75**, 184434 (2007).

[42] S. Miyasaka, J. Fujioka, M. Iwama, Y. Okimoto, Y. Tokura, *Phys. Rev. B* **73**, 224436 (2006).

[43] M. Raczkowski, A.M. Oleś, *Phys. Rev. B* **66**, 094431 (2002).

[44] M. Reehuis, C. Ulrich, P. Pattison, B. Ouladdiaf, M.C. Rheinstdter, M. Ohl, L.P. Regnault, M. Miyasaka, Y. Tokura, B. Keimer, *Phys. Rev. B* **73**, 094440 (2006).

[45] M.H. Sage, G.R. Blake, G.J. Nieuwenhuys, T.T.M. Palstra, *Phys. Rev. Lett.* **96**, 036401 (2006).

[46] M.H. Sage, G.R. Blake, C. Marquina, T.T.M. Palstra, *Phys. Rev. B* **96**, 195102 (2007).

[47] P. Horsch, A.M. Oleś, L.F. Feiner, G. Khaliullin, *Phys. Rev. Lett.* **100**, 167205 (2008).

[48] E. Pavarini, Y. Yamasaki, J. Nuss, O.K. Andersen, *New J. Phys.* **7**, 188 (2005).

[49] M. De Raychaudhury, E. Pavarini, O.K. Andersen, *Phys. Rev. Lett.* **99**, 126402 (2007).

[50] I.V. Solovyev, *J. Phys., Condens. Matter* **20**, 293201 (2008).

[51] G. Khaliullin, *Prog. Theor. Phys. Suppl.* **160**, 155 (2005).

[52] B. Normand, A.M. Oleś, *Phys. Rev. B* **78**, 094427 (2008).

[53] J. van den Brink, *Phys. Rev. Lett.* **87**, 217202 (2001).

[54] C. Ulrich, A. Gössling, M. Grüninger, M. Guennou, H. Roth, M. Cwik, T. Lorenz, G. Khaliullin, B. Keimer, *Phys. Rev. Lett.* **97**, 157401 (2006).

[55] J. Zaanen, A.M. Oleś, *Phys. Rev. B* **48**, 7197 (1993).

[56] J. Zaanen, A.M. Oleś, P. Horsch, *Phys. Rev. B* **46**, 5798 (1992).

[57] J. van den Brink, P. Horsch, A.M. Oleś, *Phys. Rev. Lett.* **85**, 5174 (2000).

[58] J. Bała, G.A. Sawatzky, A.M. Oleś, A. Macridin, *Phys. Rev. Lett.* **87**, 067204 (2001).

[59] M. Daghofer, K. Wohlfeld, A.M. Oleś, E. Arrigoni, P. Horsch, *Phys. Rev. Lett.* **100**, 066403 (2008).

[60] K. Wohlfeld, A.M. Oleś, M. Daghofer, P. Horsch, *Acta Phys. Pol. A* **115**, 110 (2009); K. Wohlfeld, A.M. Oleś, M. Daghofer, P. Horsch, *Phys. Rev. B* **78**, 214423 (2008).

[61] M. Daghofer, A.M. Oleś, *Acta Phys. Pol. A* **111**, 497 (2007).

[62] J. Fujioka, S. Miyasaka, Y. Tokura, *Phys. Rev. B* **72**, 024460 (2005).

[63] J. Fujioka, S. Miyasaka, Y. Tokura, *Phys. Rev. B* **77**, 144402 (2008).

[64] J. Chakhalian, J.W. Freeland, G. Srajer, J. Strempfer, G. Khaliullin, J.C. Cezar, T. Charlton, R. Dalgliesh, C. Bernhard, G. Cristiani, H.U. Habermeier, B. Keimer, *Nature Phys.* **2**, 244 (2006).

[65] J. Chaloupka, G. Khaliullin, *Phys. Rev. Lett.* **100**, 016404 (2008).

[66] F. Mack, P. Horsch, *Phys. Rev. Lett.* **82**, 3160 (1999).